

Detectability Scaling Laws for Environmental Phase Modulation in Gravitational-Wave Signals

Jericho Cain*

Physics Department, Portland Community College, Portland, OR, USA

(Dated: March 16, 2026)

Environmental effects such as hierarchical triple motion introduce cumulative phase modulation in gravitational-wave signals through time-dependent line-of-sight acceleration. Whether such effects are observable depends on both deformation strength and signal-to-noise ratio (SNR). However, this relationship has not been quantified in a waveform-agnostic manner. Here we investigate the detectability of smooth time-warp distortions using template-free time–frequency representations. Rather than relying on direct strain-domain residuals, we analyze trajectory-level statistics derived from the continuous wavelet transform, in particular the evolution of the power-weighted frequency centroid. We show that environmental modulation can be detected using a single-sample statistic referenced to an isolated-binary distribution, without requiring matched templates. Across a grid of cumulative phase distortions $\Delta\phi$ and SNR, the detection performance collapses onto a single scaling parameter, $\Lambda = \Delta\phi \times \text{SNR}$. The ROC-AUC follows an approximately sigmoid curve in Λ with a clear transition region. For moderate distortions ($\Delta\phi \gtrsim 3$ rad), environmental modulation is detectable even at low SNR. For smaller distortions ($\Delta\phi \sim 1$ rad), detectability is noise-limited and emerges only at $\text{SNR} \gtrsim 20$. Within the controlled waveform family studied here, smooth environmental phase modulation is not generically absorbed by intrinsic waveform variability. Instead, detectability is governed by a simple scaling between cumulative phase distortion and signal strength. This scaling relation provides a concrete reference point for template-free environmental searches in gravitational-wave data.

I. INTRODUCTION

Many massive stars reside in multiple systems. Observation has shown that high mass stars, like O-type, are found predominately in multiple systems [1] and a good chunk of those exist in triples or higher, more so with increasing mass [2]. The systems with three stars are called hierarchical triple systems (HTS) and are important for gravitational wave detection.

Matched filtering using waveform templates representing binary systems have been used successfully for detection and parameter estimation [3]. However, HTS change gravitational waveforms systematically. Similar phase distortions can arise from other large-scale environmental accelerations, making it useful to understand their detectability in a waveform-agnostic framework. For HTS motion, the inner binary about a tertiary companion induces a time-dependent line-of-sight acceleration (LOSA) [4, 5] and structured acceleration profiles can produce nontrivial phase evolution beyond constant-acceleration approximations [6, 7]. This can create phase modulation that accumulates over time producing cumulative phase drift. If in detection we assume the source is an isolated binary, but the system is an HTS, this phase drift may be absorbed into intrinsic parameters biasing estimations of mass, chirp rate, or spin. In other words, the LOSA signal stays inside the isolated binary envelope hidden through incorrect parameter estimation – the effect is degenerate.

We therefore ask whether environmental phase modulation can be detected without constructing explicit environmental waveform templates. In this work we show that the detectability of such distortions obeys a simple scaling relation governed by the product of cumulative phase deformation and signal-to-noise ratio. In particular, receiver operating characteristic (ROC) performance collapses onto a single parameter $\Lambda = \Delta\phi_{env} \times \text{SNR}$. Using time–frequency representations computed from continuous wavelet transforms (CWT), we demonstrate this scaling by analyzing trajectory-level statistics derived from the power-weighted frequency centroid of the signal. Detection performance remains near chance below a characteristic value of Λ , and rises rapidly above it. In particular, phase distortions $\Delta\phi \gtrsim 3$ rad are detectable even at low SNR, but $\Delta\phi \sim 1$ rad becomes observable only when $\text{SNR} \gtrsim 20$.

LOSA distortions produce measurable shifts in centroid trajectories that follow predictable $\text{SNR}-\Delta\phi$ scaling. This relation provides a physically interpretable baseline for template-free environmental searches in current and future gravitational-wave detectors.

II. WAVEFORM MODEL AND ENVIRONMENTAL PHASE MODULATION

A. Isolated Chirp Model

To isolate the time-reparameterization effect under controlled statistical conditions we begin with a minimal inspiral-like chirp model. The same deformation behavior is also demonstrated using a post-Newtonian inspiral

* jericho.cain@gmail.com

waveform.

$$h_{\text{iso}}(t) = A(t) \cos[\phi_{\text{iso}}(t)], \quad (1)$$

where $A(t)$ is a smooth amplitude envelope and $\phi_{\text{iso}}(t)$ is a monotonically increasing phase. The instantaneous frequency is

$$f_{\text{iso}}(t) = \frac{1}{2\pi} \frac{d\phi_{\text{iso}}}{dt}. \quad (2)$$

For concreteness, we employ a Gaussian-modulated chirp with frequency evolving from f_{start} to f_{end} over the signal duration. The precise functional form is not critical; what matters is that $f_{\text{iso}}(t)$ is smooth and increasing, mimicking the qualitative structure of compact-binary inspiral.

B. Line-of-Sight Acceleration as a Time Warp

Environmental motion induces a detector-frame time reparameterization. If the source experiences line-of-sight acceleration, the observed signal becomes

$$h_{\text{LOSA}}(t) = h_{\text{iso}}(t + \Delta t(t)), \quad (3)$$

where $\Delta t(t)$ is a smooth, slowly varying time shift determined by the relative motion of the source.

In the constant-acceleration approximation,

$$\Delta t(t) = \frac{a_{\parallel}}{c} \frac{t^2}{2}, \quad (4)$$

where a_{\parallel} is the line-of-sight acceleration and c is the speed of light. More general acceleration profiles yield correspondingly smooth $\Delta t(t)$ functions.

This deformation is purely kinematic. The intrinsic phase evolution remains unchanged, but it is evaluated at a shifted time coordinate. The strain-domain difference

$$\Delta h(t) = h_{\text{LOSA}}(t) - h_{\text{iso}}(t) \quad (5)$$

can be visually small even when the cumulative phase distortion is significant.

C. Cumulative Phase Distortion

The observable effect of LOSA is best characterized by the cumulative phase difference between the deformed and isolated signals,

$$\Delta\phi(t) = \phi_{\text{iso}}(t + \Delta t(t)) - \phi_{\text{iso}}(t). \quad (6)$$

For small time shifts,

$$\Delta\phi(t) \approx 2\pi f_{\text{iso}}(t) \Delta t(t). \quad (7)$$

We define the total environmental phase distortion

$$\Delta\phi = \max_t |\Delta\phi(t)|, \quad (8)$$

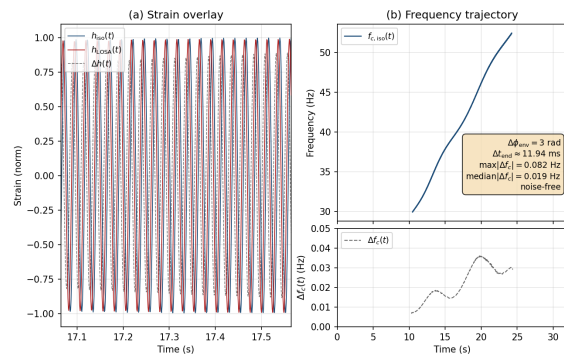


FIG. 1. Environmental phase modulation for $\Delta\phi = 3$ rad (noise-free). (a) Zoomed strain overlay showing the isolated chirp $h_{\text{iso}}(t)$ (blue) and the LOSA-deformed signal $h_{\text{LOSA}}(t)$ (red) during the final ~ 0.5 s prior to peak strain. The dashed curve shows the strain difference $\Delta h(t) = h_{\text{LOSA}} - h_{\text{iso}}$. (b) Time-frequency centroid trajectory and its deviation, which will be defined formally in Sec. III B.

which serves as a convenient one-parameter measure of deformation strength.

In our controlled experiments, $\Delta\phi$ is varied systematically while keeping the intrinsic waveform fixed. For example, $\Delta\phi = 3$ rad corresponds to an end-of-signal time shift of order ~ 10 ms for the fiducial chirp used here.

D. Effect on Instantaneous Frequency

Because the deformation is a time warp, the instantaneous frequency of the observed signal becomes

$$f_{\text{LOSA}}(t) = \frac{1}{2\pi} \frac{d}{dt} \phi_{\text{iso}}(t + \Delta t(t)). \quad (9)$$

Expanding to first order,

$$f_{\text{LOSA}}(t) \approx f_{\text{iso}}(t) + \dot{\Delta t}(t) f_{\text{iso}}(t) + \Delta t(t) \dot{f}_{\text{iso}}(t). \quad (10)$$

Thus LOSA induces a smooth deviation in the frequency trajectory, even when the strain-domain difference appears visually subtle. It is this trajectory-level distortion that we quantify in the subsequent sections.

To illustrate the structure of the LOSA-induced deformation, we show in Fig. 1 a representative Gaussian-modulated chirp example with $\Delta\phi = 3$ rad in the noise-free limit. Panel (a) displays a zoomed view of the final ~ 0.5 s prior to peak strain in order to resolve the oscillatory phase structure. The LOSA time reparameterization produces a cumulative multi-radian phase slip that appears as a progressive offset between the isolated and deformed waveforms. Despite the several-radian cumulative distortion, the strain-domain amplitude remains nearly unchanged. This illustrates that LOSA acts primarily as a smooth time warp rather than as an amplitude modulation.

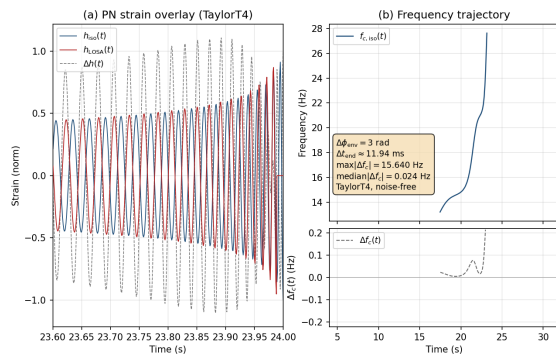


FIG. 2. Environmental phase modulation applied to a post-Newtonian (TaylorT4) inspiral waveform with $\Delta\phi = 3$ rad (noise-free). (a) Zoomed strain overlay during the final ~ 0.4 s before merger. The LOSA-deformed signal (red) exhibits a cumulative phase slip relative to the isolated waveform (blue); the dashed curve shows the strain difference $\Delta h(t)$. (b) Corresponding time–frequency centroid trajectory $f_c(t)$ (top) and its deviation $\Delta f_c(t)$ (bottom). The deformation appears as a coherent modification of the centroid evolution, consistent with a smooth time reparameterization rather than a constant phase offset.

To demonstrate that this behavior persists for physically motivated waveforms, we apply the LOSA time reparameterization to a post-Newtonian inspiral generated using the TaylorT4 approximation. Figure 2(a) shows a representative example with cumulative phase distortion $\Delta\phi = 3$ rad in the noise-free limit. As in the Gaussian case, the deformation manifests primarily as a progressive phase slip rather than as a large amplitude discrepancy. This reflects the fact that LOSA does not alter the intrinsic binary dynamics; instead, it smoothly warps the time coordinate.

For completeness, both figures also display in panel (b) the corresponding deformation in a time–frequency representation. These quantities will be defined formally in Sec. III B.

In the controlled detectability experiments that follow, we employ the Gaussian-modulated chirp model introduced above to isolate the deformation mechanism under well-defined statistical conditions. The post-Newtonian example demonstrates that the same trajectory-level distortion arises for physically motivated inspiral waveforms.

III. EXPERIMENTAL DESIGN

The goal of this study is to determine when environmental phase modulation becomes statistically observable in noisy data. We treat detectability as a function of two independent controls: the cumulative environmental phase distortion $\Delta\phi$ and the signal-to-noise ratio (SNR). Rather than relying on template matching or reconstruc-

tion error, we evaluate a single-sample statistic defined relative to a reference distribution of isolated signals.

A. Synthetic Signal Generation

We generate quasi-monochromatic inspiral-like chirp signals with frequency evolution spanning 12–65 Hz over a 32 s duration. The strain is tapered with a Gaussian envelope to suppress boundary artifacts. Environmental modulation is introduced as a smooth time reparameterization,

$$h_{\text{LOSA}}(t) = h_{\text{iso}}(t + \Delta t(t)), \quad (11)$$

where $\Delta t(t)$ corresponds to constant line-of-sight acceleration in the perturbative regime.

The deformation strength is characterized by the cumulative phase shift

$$\Delta\phi = \max_t |\phi_{\text{LOSA}}(t) - \phi_{\text{iso}}(t)|. \quad (12)$$

Unless otherwise specified, signals are embedded in stationary Gaussian noise for statistical evaluation, while noise-free injections are used for visual diagnostics.

Detectability is evaluated on a controlled grid of

$$\Delta\phi \in \{0.3, 1, 3\} \text{ rad} \quad \text{and} \quad \text{SNR} \in \{5, 10, 20, 40\}.$$

Additional larger distortions are used for diagnostic checks. For each $(\Delta\phi, \text{SNR})$ pair, isolated and LOSA-modulated samples are generated independently with distinct noise realizations. No pairing or oracle reference is used in the primary statistical evaluation.

B. Detection Statistic

Time–frequency representations are computed using the continuous wavelet transform. From the power spectrum $P(f, t)$, we extract the power-weighted frequency centroid

$$f_c(t) = \frac{\sum_k f_k P_{k,t}}{\sum_k P_{k,t}}, \quad (13)$$

restricted to gated time bins.

The time–frequency centroid $f_c(t)$ corresponds to the upper panel (b) in Figs. 1 and 2.

A reference trajectory $\mu_{\text{iso}}(t)$ is constructed by averaging $f_c(t)$ over an ensemble of isolated training signals. For each evaluation sample (isolated or LOSA-modulated), we compute the scalar score

$$S_{f_c} = \text{median}_t |f_c(t) - \mu_{\text{iso}}(t)|. \quad (14)$$

This statistic measures deviation from the isolated centroid trajectory without access to the true isolated counterpart.

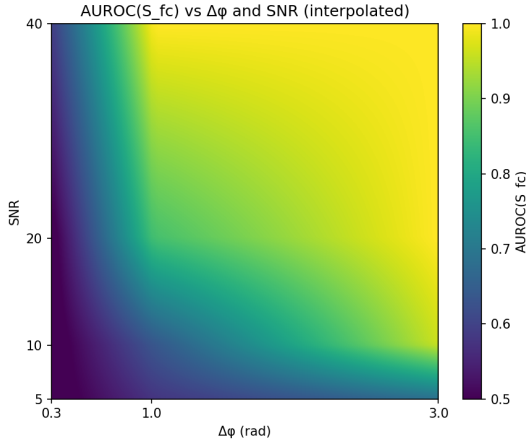


FIG. 3. AUROC as a function of cumulative phase distortion $\Delta\phi$ and SNR. Detectability increases with both deformation strength and signal amplitude.

Detection performance is quantified using receiver operating characteristic (ROC) curves comparing isolated and LOSA samples. For each grid point, the area under the ROC curve (AUROC) is computed using S_{fc} as the ranking statistic.

C. Scaling Analysis

To assess whether detectability obeys a single-parameter control, we define the composite variable

$$\Lambda = \Delta\phi \times \text{SNR}. \quad (15)$$

AUROC values from the full $(\Delta\phi, \text{SNR})$ grid are analyzed as a function of Λ . This allows us to test for collapse onto a universal curve and to characterize the transition between degenerate and separable regimes via a sigmoid fit.

IV. RESULTS

A. Detectability Surface in SNR and Cumulative Phase Distortion

Figure 3 shows AUROC as a function of cumulative phase distortion $\Delta\phi$ and signal-to-noise ratio (SNR). Each grid point represents an independent evaluation using the centroid-deviation statistic S_{fc} .

Several features are immediately apparent:

- For $\Delta\phi \approx 0.3$ rad, detectability remains near chance across most SNR values.
- For $\Delta\phi \approx 1$ rad, detection emerges at $\text{SNR} \gtrsim 20$.
- For $\Delta\phi \approx 3$ rad, environmental modulation is detectable even at $\text{SNR} \approx 5$.

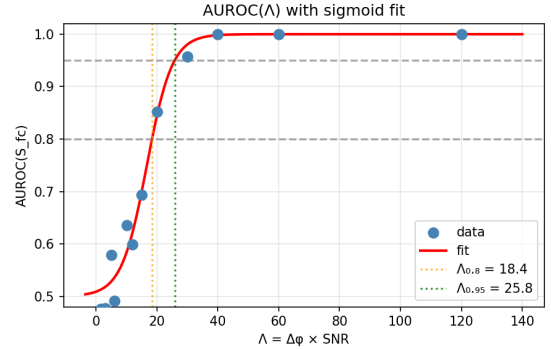


FIG. 4. AUROC as a function of the composite parameter $\Lambda = \Delta\phi \times \text{SNR}$. Points from all $(\text{SNR}, \Delta\phi)$ combinations collapse onto a single curve, demonstrating one-parameter scaling of environmental detectability. The red curve shows a sigmoid fit to the collapsed data. Vertical lines indicate characteristic threshold values corresponding to AUROC = 0.8 and 0.95.

These results indicate that detectability is jointly controlled by deformation strength and signal amplitude. Neither parameter alone determines observability.

B. Single-Parameter Scaling and Sigmoid Transition

Figure 4 shows AUROC plotted against Λ for all measured grid points. The collapse is striking: data from different SNR and deformation combinations align along a common monotonic trajectory. This indicates that detectability is governed by the product $\Delta\phi \times \text{SNR}$, rather than by either parameter independently.

To quantify the transition, we fit the scaling curve with a sigmoid model

$$\text{AUROC}(\Lambda) = 0.5 + \frac{0.5}{1 + \exp[-k(\Lambda - \Lambda_0)]}. \quad (16)$$

The offset of 0.5 reflects the fact that chance performance for a balanced binary classification test corresponds to AUROC = 0.5. Figure 4 shows the fitted curve along with threshold levels corresponding to AUROC = 0.8 and AUROC = 0.95.

The fitted parameters yield a well-defined transition scale Λ_0 . Detection probability increases rapidly once Λ exceeds this threshold, indicating a sharp transition between noise-dominated and signal-dominated regimes.

C. Time-Local Behavior of the Centroid Shift

To verify that the centroid-based statistic reflects a physically meaningful deformation rather than a numerical artifact, we examine the explicit time evolution of the centroid difference

$$\Delta f_c(t) = f_{c,\text{LOSA}}(t) - f_{c,\text{iso}}(t), \quad (17)$$

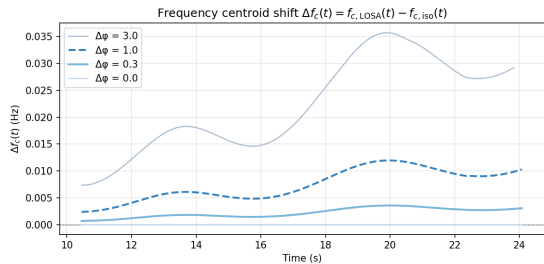


FIG. 5. Time evolution of the centroid shift $\Delta f_c(t)$ for representative cumulative phase distortions. Larger $\Delta\phi$ produces systematically larger centroid deviations, while preserving the characteristic smooth temporal structure.

for representative deformation strengths. This quantity corresponds to the lower panel (b) in Figs. 1 and 2, where a single example with $\Delta\phi = 3$ rad was shown. In Fig. 5, we extend that visualization across multiple cumulative phase distortions to examine the scaling behavior of the centroid deviation.

As the cumulative phase distortion increases, the magnitude of $\Delta f_c(t)$ grows smoothly and systematically. The deviation exhibits coherent time structure rather than random fluctuations, confirming that the statistic tracks the expected time-warp deformation of the chirp trajectory. This behavior is consistent with the interpretation developed in Sec. II: LOSA acts as a smooth reparameterization of time, which manifests as a structured distortion of the time–frequency centroid trajectory.

D. Physical Interpretation

The scaling behavior can be understood intuitively. The cumulative phase distortion $\Delta\phi$ sets the magnitude of the trajectory deformation, while SNR sets the inverse noise floor against which that deformation is measured. Their product therefore determines the effective signal-to-distortion ratio in the centroid trajectory.

Within the controlled waveform family studied here, environmental phase modulation does not appear to be intrinsically degenerate with intrinsic variability in the centroid representation. Instead, observability is governed by a quantitative scaling relation in Eq. (15). Below the transition scale, noise fluctuations dominate centroid deviations. Above it, deformation-induced structure becomes statistically resolvable.

V. DISCUSSION

A. Physical Interpretation of the Scaling Law

The collapse observed in Sec. IV suggests Λ functions as an effective signal-to-distortion ratio in the centroid trajectory. This scaling can be understood using simple

phase-measurement arguments. Environmental acceleration produces a deterministic cumulative phase distortion of magnitude $\Delta\phi_{\text{env}}$. In gravitational-wave parameter estimation, the uncertainty with which waveform phase can be measured scales approximately as $\sigma_\phi \sim 1/\text{SNR}$. Detectability therefore depends on the ratio between deformation amplitude and measurement uncertainty, yielding an effective signal-to-distortion parameter proportional to $\Delta\phi_{\text{env}} \times \text{SNR}$. The numerical experiments presented here confirm that ROC performance collapses onto this expected scaling. Across the explored grid of cumulative phase distortions and signal-to-noise ratios, AUROC values collapse onto a single sigmoid curve when plotted against Λ .

This behavior has a direct physical interpretation. Line-of-sight acceleration induces a smooth time reparameterization, which in turn produces a systematic deviation in the time–frequency trajectory of the signal. In the perturbative regime, the magnitude of this trajectory shift scales approximately linearly with $\Delta\phi$. Measurement uncertainty in the centroid trajectory decreases with increasing SNR. Detectability is therefore controlled by the ratio between deterministic deformation amplitude and stochastic measurement noise, naturally leading to the product scaling in Eq. (15).

The sigmoid transition reflects the crossover between noise-dominated and deformation-dominated regimes. For $\Lambda \ll \Lambda_0$, LOSA-induced distortions are indistinguishable from statistical fluctuations. For $\Lambda \gg \Lambda_0$, the deformation dominates trajectory noise and separability approaches unity.

The primary contribution of this work is therefore the identification of this simple detectability scaling in $\Lambda = \Delta\phi_{\text{env}} \times \text{SNR}$, while the centroid-based statistic used here serves as a representative trajectory diagnostic for demonstrating the effect.

B. Noise-Limited Versus Physics-Limited Regimes

The detectability surface indicates that weak environmental distortions are not fundamentally hidden by intrinsic waveform structure. Instead, observability is noise-limited at small $\Delta\phi$.

For moderate distortions ($\Delta\phi \gtrsim 3$ rad), detectability remains high even at modest SNR. For smaller distortions ($\Delta\phi \sim 1$ rad), separation improves rapidly with increasing SNR, becoming reliable only once Λ exceeds threshold. Thus the limiting factor in the weak-deformation regime is statistical precision rather than representational degeneracy.

C. Practical Use in Detection Pipelines

The scaling law derived here does not replace matched filtering, but it suggests a complementary diagnostic layer for environmental searches. After a standard binary

detection, one may construct a time-frequency representation of the recovered strain and evaluate the centroid-based statistic S_{fc} relative to an isolated reference distribution. The inferred value of Λ provides a quantitative criterion for whether environmental time reparameterization is statistically resolvable.

Such a statistic could serve as a lightweight screening tool, flagging events that warrant hierarchical or acceleration-aware waveform modeling. Conversely, in low-SNR regimes where Λ is below threshold, the analysis indicates that environmental signatures are unlikely to be recoverable without additional information. Beyond individual events, stacking centroid deviations across populations may provide a statistical probe of environmental effects even when single-event detectability is marginal.

The centroid-based statistic introduced here is also compatible with representation-learning frameworks in which compact-binary signals occupy a low-dimensional manifold in time-frequency space. If the latent representation preserves the time-frequency trajectory geometry, LOSA-induced deformation would correspond to a systematic displacement from the isolated manifold. Template-free autoencoder models trained on isolated binaries, such as [8], could therefore flag environmental modulation as a structured anomaly rather than generic noise. This suggests a natural extension in which the present scaling law is used to calibrate latent-space environmental sensitivity.

D. Implications for Current and Future Detectors

From the fitted sigmoid in Sec. IV, we obtain characteristic thresholds

$$\Lambda_{0.8} \approx 19, \quad \Lambda_{0.95} \approx 27,$$

corresponding to AUROC values of 0.8 and 0.95.

For ground-based detectors such as Advanced LIGO and Virgo, typical binary black hole events have network SNR ~ 8 –20. At SNR ≈ 10 , the condition $\Lambda \gtrsim 20$ implies that cumulative phase distortions of order $\Delta\phi \gtrsim 2$ rad are required for robust detectability. For louder events with SNR ≈ 20 , the threshold relaxes to $\Delta\phi \gtrsim 1$ rad.

Space-based detectors such as LISA operate in a different regime. Long-duration inspirals in the milli-Hz band can accumulate very high SNR over months to years of observation. In that limit, even comparatively small cumulative phase distortions may satisfy $\Lambda \gtrsim 20$. Environmental time-warp effects that are marginal in current ground-based observations could therefore become observable in high-SNR space-based measurements.

E. Limitations and Future Work

The present analysis employs controlled chirp families and a simplified constant-acceleration model in order to isolate the time-reparameterization effect under well-defined statistical conditions. Environmental acceleration acts primarily as a smooth time warp, producing a cumulative phase deformation without strongly altering the amplitude structure of the waveform. Because this deformation is determined primarily by the accumulated phase shift $\Delta\phi_{\text{env}}$, the detectability scaling with $\Lambda = \Delta\phi_{\text{env}} \times \text{SNR}$ is expected to hold for any smoothly evolving inspiral waveform. The post-Newtonian TaylorT4 example shown in Fig. 2 illustrates that the same trajectory-level distortion arises for physically motivated gravitational-wave signals.

Real hierarchical triple systems can produce time-dependent accelerations beyond quadratic time shifts, and realistic compact-binary waveforms contain additional structure absent from the simplified model considered here.

Future work should extend the scaling analysis to post-Newtonian inspiral waveforms and astrophysically motivated acceleration profiles. Alternative trajectory statistics sensitive to higher-order curvature in time–frequency space may further reduce detection thresholds.

Nevertheless, within the controlled framework studied here, environmental phase modulation exhibits a simple observability scaling law governed by Eq. (15). Detectability is controlled by the interplay between cumulative phase distortion and signal strength, rather than by a fundamental degeneracy with intrinsic waveform structure.

-
- [1] H. Sana, S. E. de Mink, A. de Koter, N. Langer, C. J. Evans, M. Gieles, E. Gosset, R. G. Izzard, J.-B. Le Bouquin, and F. R. N. Schneider, *Science* **337**, 444 (2012).
 - [2] C. Shariat, K. El-Badry, and S. Naoz, *Publications of the Astronomical Society of the Pacific* **137**, 094201 (2025).
 - [3] N. Christensen and R. Meyer, *Reviews of Modern Physics* **94**, 025001 (2022).
 - [4] P. Gupta, H. Suzuki, H. Okawa, and K.-i. Maeda, *Physical Review D* **101**, 104053 (2020).
 - [5] V. Cardoso, F. Duque, and G. Khanna, *Physical Review D* **103**, l081501 (2021).
 - [6] K. Hendriks, L. Zwick, P. Saini, J. Takátsy, and J. Samsing, *Towards gravitational wave parameter inference for binaries with an eccentric companion* (2026), arXiv:2601.14918 [astro-ph.HE].
 - [7] L. Zwick, P. R. Capelo, and L. Mayer, *Monthly Notices of the Royal Astronomical Society* **521**, 4645 (2023).
 - [8] J. E. Cain, *Classical and Quantum Gravity* 10.1088/1361-6382/ae415e (2026).